nature geoscience

ARTICLES

PUBLISHED ONLINE: 10 JULY 2017 | DOI: 10.1038/NGEO2982

A reverse energy cascade for crustal magma transport

Leif Karlstrom[1]*, Scott R. Paterson[2] and A. Mark Jellinek[3]

Direct constraints on the ascent, storage and eruption of mantle melts come primarily from exhumed, long-frozen intrusions. These structures, relics of a dynamic magma transport network, encode how Earth's crust grows and differentiates over time. Furthermore, they connect mantle melting to an evolving distribution of surface volcanism. Disentangling magma transport processes from the plutonic record is consequently a seminal but unsolved problem. Here we use field data analyses, scaling theory and numerical simulations to show that the size distribution of intrusions preserved as plutonic complexes in the North American Cordillera suggests a transition in the mechanical response of crustal rocks to protracted episodes of magmatism. Intrusion sizes larger than about 100 m follow a power-law scaling expected if energy delivered from the mantle to open very thin dykes and sills is transferred to intrusions of increasing size. Merging, assimilation and mixing of small intrusions into larger ones occurs until irreversible deformation and solidification dissipate available energy. Mantle magma supply over tens to hundreds of thousands of years will trigger this regime, a type of reverse energy cascade, depending on the influx rate and efficiency of crustal heating by intrusions. Identifying regimes of magma transport provides a framework for inferring subsurface magmatic processes from surface patterns of volcanism, information preservation in the plutonic record, and related effects including climate.

Most magma ascending into the crust stalls and crystallizes prior to reaching the surface[1,2]. Although this crustal filter plays a fundamental role in the thermal and climatic histories of Earth and other planets[3], it is not known precisely why so little magma is erupted in long-lived volcanic provinces, or how such low eruption efficiency relates to the rheology and evolving structure of crust that supports active magmatism[4]. Mechanics of intrusion growth and connections to surface volcanism have been historically challenging to address. The spatially and temporally complex character of intrusions is related, in part, to prolonged incremental assembly[5,6], and obscures observational clues about the dynamics of magma transport through time. Nevertheless, there is an expansive spatial record of frozen intrusions exposed in terrains from all levels of the crust. Consequently, there is an outstanding need for overarching theory to connect these data with constraints from active intrusions[7].

The response of crustal rocks to injections of mantle melt spans a continuum among elastic, brittle, plastic and viscous behaviour[8]. For example, dykes are reasonably well characterized as magma-filled fractures, such that dyke widths encode flux rates, magma viscosity and crustal strength[9–11]. Despite ambiguity between frozen and active structures, the relatively narrow range of dyke widths observed (Fig. 1a) suggests a consistent physical origin. In contrast, plutonic body dimensions vary widely and appear self-similar at scales above ∼1 km (ref. 12). Complete size distributions are challenging as mechanical boundaries between intrusions are often difficult to identify rigorously and laborious to extract, limiting the scope of previous theoretical work on the incremental growth model[13,14] or growth of intrusions[15–17].

Plutonic intrusion sizes suggest distinct process regimes

Motivated by previous field observations[18,19] and compilations[12], we present new data that offer unprecedented detail on intrusion shapes and sizes from the North American Cordillera. Within plutonic complexes we identify two modes of intrusion morphology: thin, texturally homogeneous sheet-like intrusions marked by sharply defined contacts with host crustal rocks; and volumetrically larger, relatively equant intrusions with spatially complex internal contacts. Although they are readily defined in rock outcrops, thin sheets are best preserved in marginal zones of plutonic complexes and often recycled or amalgamated into larger bodies[19,20]. This merging and mechanical mixing of small intrusions into plutons contributes to their incremental growth[21] and internal magmatic deformation, which is expressed as textural and mineral chemical heterogeneity[22,23].

Figure 1 plots the size distribution of intrusions characterized by their minimum dimension inferred from outcrop, plotted as wavenumber k (inverse length, bottom axis) and wavelength (top axis). We use a single minimum dimension rather than other possible choices of scale length as this parameter sets intrusion aspect ratio and facilitates comparison with dykes[10], which govern the input of mantle melts into the crust. The thinnest intrusions from arc complexes overlap with dykes from oceanic island settings and flood basalts, but are clearly distinguished from larger bodies within plutonic complexes (Fig. 1a). Figure 1b is a subset of ten particularly well-studied complexes (green bars, Methods). For these sites, the complete distribution of intrusions sizes from the smallest recorded to the final composite complexes exhibits an inverse relationship between intrusion number density and scale length.

The distinct morphologic classes of intrusions suggest variable mechanical responses of crustal rocks to a given regional magma supply. Thin sheets, dykes and sills are consistent with a plastic or brittle response to forced magma injections that open cracks faster than restoring viscous host-rock creep can operate[24]. Intrusions in this rheological regime are restricted to high-aspect-ratio geometries, propagating according to the characteristics of the magmatic driving stress, regional stresses, and mechanical heterogeneity or plastic response of host rocks[25–27]. By contrast, where the speed of

[1]Department of Earth Sciences, University of Oregon, Eugene, Oregon 97403, USA. [2]Department of Earth Sciences, University of Southern California, Los Angeles, California 90089, USA. [3]Department of Earth, Ocean and Atmospheric Sciences, The University of British Columbia, British Columbia V6T 1Z4, Canada. *e-mail: leif@uoregon.edu

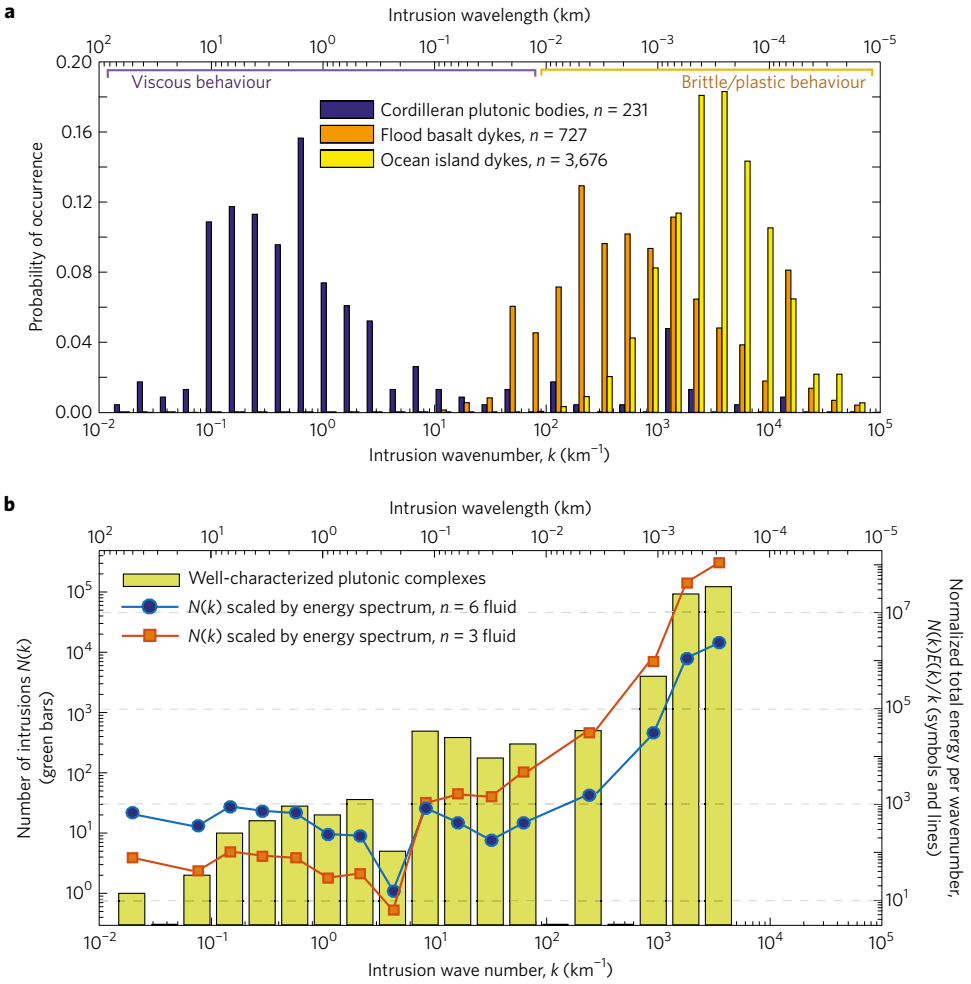

Figure 1 | Normalized histograms of characteristic length scales associated with magmatic intrusions. a, Dykes (yellow bars from oceanic settings[11], orange bars from flood basalt provinces[47,48], Methods) and North American plutonic complexes (blue bars, this study), with the top scale being the minimum intrusion dimension, and the bottom scale its inverse (wavenumber k); the measurements are described in the text. Labelled 'viscous' and 'brittle/plastic' regimes of host-rock response indicate control on intrusion sizes. **b**, Number density of plutonic bodies $N(k)$, scaling average measurements to their map area (green bars, left-hand scale). Symbols and lines plot $N(k)$ multiplied by normalized energy per wavenumber from equation (1) (right-hand scale), for two choices of fluid power-law exponent ($n = 3$ and $n = 6$). $N(k)E(k)/k$ is approximately constant over a wide range of k, consistent with a steady-state, self-similar energy cascade.

viscous deformation exceeds the rate of elastic deformation within warm or highly damaged host rocks, reservoir size is restricted spatially primarily by influx, leading to development in some cases of large storage zones that feed caldera-forming eruptions[15].

Prevalence of intrusions within the elastic regime across tectonic settings indicates that energy input to the crustal magma transport system occurs primarily at small length scales ($\sim 10^2 < k < 10^5$ km^{-1}, Fig. 1a)[24,28]. We hypothesize that the power-law intrusion distribution in Fig. 1b records, in part, a self-similar mechanical transfer of melt input at small scales to larger intrusions that is possible only after sufficient warming occurs. Elastic work extracted from mantle influx to open and propagate small sheets is transferred continuously to larger scales and ultimately dissipated through mixing and merging of intrusions as well as their cooling and solidification. Sinks of energy from hydrothermal circulation and passive degassing of exsolved volatiles participate depending on the depth[29]. Energy is also lost irreversibly to surface volcanism. However, if the fraction of injected magma erupted at the surface (the eruption efficiency) is low[2], the contribution of this sink to the total rate at which energy supplied from the mantle is dissipated is negligible.

Implicit in this phenomenological model are three assumptions. The first assumption is that the intrusion-scale separation suggested in Fig. 1a will occur where the host-rock response to an imposed regional magma supply transitions from being predominantly elastic (Fig. 2a) to viscous (Fig. 2b), on average. Quantitatively, the mechanical response of the crust to injected magma is characterized by a Deborah number $\mathrm{De} = T_{\mathrm{relax}}/T_{\mathrm{inject}}$, which compares an injection timescale T_{inject} with the stress relaxation timescale T_{relax} (ref. 15). Whereas T_{inject} scales with the size of crustal intrusions relative to the influx rate, T_{relax} scales with an effective elastic modulus and crustal viscosity, which depends strongly on temperature and accumulated damage[30,31], as well as reservoir geometry and depth[17].

A second assumption is that the spectrum of intrusion sizes in Fig. 1 is a steady-state property of the crustal response. This scenario is possible only in sufficiently heated crust, because $\mathrm{De} \gg 1$ intrusions are restricted to very small scales (Fig. 1a). Mantle melt influx is, however, probably unsteady[32], so the time to reach a $\mathrm{De} < 1$ condition depends on the long-term average influx as well as its temporal variability. The extent to which intermittency in the magma supply matters may be estimated by comparing the timescale for variations in mantle supply T_{supply} with the timescale for thermal diffusion $T_{\mathrm{diffusion}}$ (ref. 33) over which heat supply fluctuations relax to the background crustal steady state. Accordingly, we define a

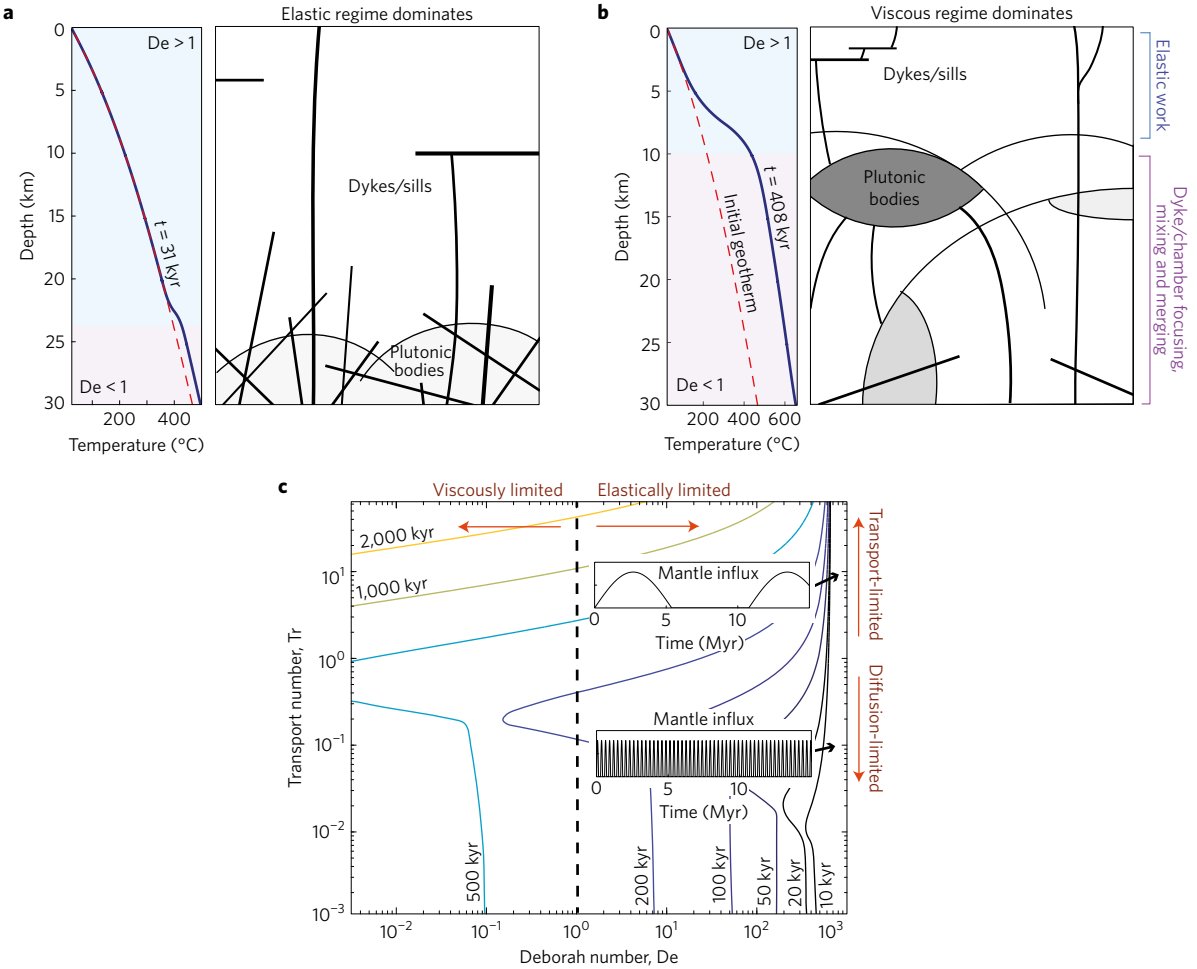

Figure 2 | Magma transport regimes are controlled by crustal rheology and episodicity of mantle melt supply. a, Elastic/brittle/plastic rheology dominates the crust, resulting in thin intrusion geometries. Deborah number distribution (De) is calculated from a model for diffusion-limited (Tr $\ll 1$) magmatic heat supply to the lowest 5 km of crust (Methods), with $Q_{in} = 10^{-3}$ km^3 yr^{-1}. **b**, Viscous (De < 1) rheology dominates, and intrusions injected throughout the lowest 15 km of crust form a steady-state network of reservoirs with a power-law size distribution. **c**, Regime diagram of intrusion style for average mantle influx of 10^{-3} km^3 yr^{-1} and intrusion domain from **b**. Time evolution for a particular periodic mantle supply rate (governed by transport number, Tr) is contoured. More episodic mantle supply results in longer times until De < 1, with long repose intervals between mantle melt inputs (inset plots).

transport number $\mathrm{Tr} = T_{\mathrm{supply}}/T_{\mathrm{diffusion}}$, where $\mathrm{Tr} \gg 1$ corresponds to transport-limited thermal evolution, while $\mathrm{Tr} \ll 1$ is diffusion-limited and indistinguishable from steady influx. If advection of heat via magmatically or meteorically derived fluids dominates heat conduction, this would set the transport number. Such a case is not explored here. Calculations for plausible Tr suggest that De ≤ 1 locally and regionally over timescales of order tens to hundreds of thousands of years (Fig. 2c, Methods). Taken together, the De — Tr regime controls intrusion shape and size, whether a continuous exchange of magma from smaller to larger scales will occur, and whether this exchange will remain self-similar. Critically, a single control parameter is responsible for intrusion regime shifts: the rate of crustal heating. Differences in setting (tectonic environment, crustal thickness) will manifest as controls on De and Tr. Our third assumption is that the power-law distribution of intrusion sizes suggested by data in Fig. 1b faithfully records the magma transport processes that govern exchange of energy from thin, elastically limited intrusions to larger bodies.

Crustal magma transport as a reverse energy cascade

With these three assumptions, the De $\ll 1$ regime of magma transport is a 'reverse energy cascade', illustrated in Fig. 3: energy input at small scales is mechanically transmitted to larger scales where it is ultimately dissipated through irreversible deformation of crustal rocks and solidification. Assuming the rate of dissipation Φ is equal to the rate at which energy is supplied to do the work of opening and propagating sheets, on dimensional grounds the energy E contained within each intrusion of scale $1/k$ will follow a generic scaling of the form[34] $E(k)/k \sim \Phi(k)^a k^b$, with $a = 2/3$, $b = -5/3$. Energy is carried up a 'transport range' with spectral slope that depends on the mechanisms governing the dissipation rate.

Consideration of processes important for $\Phi(k)$ (Methods) leads to the energy spectrum

$$\frac{E(k)}{k} \sim (C_M k^{3(\frac{1}{n}+1)} + C_T k)^{2/3} k^{-5/3} \quad (1)$$

where C_M and C_T are independent of wavenumber and a crustal rheology is assumed in which applied deviatoric stresses are proportional to the rate of deformation to the power $1/n$. Increasing n results in progressively localized deformation zones for given applied stresses; typical crustal and lithospheric rocks lie in the range $2 \leq n \leq 10$ (Methods). Equation (1) predicts that the spectral slope of the reverse energy cascade varies with intrusion size. For small intrusions mechanical dissipation through plastic and brittle processes dominates (larger n models correspond to the increasingly localized deformation indicative of a brittle response[35]), but this mechanism becomes less important compared with dissipation by solidification as intrusions become large. A crossover wavenumber

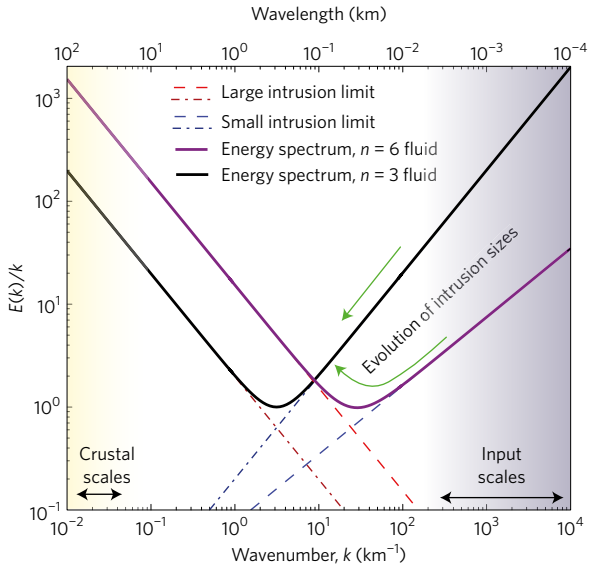

Figure 3 | A magmatic reverse energy cascade in the viscous regime. Energy spectrum of De ≪ 1 intrusions from equation (1), for two possible fluid power-law exponents. Curves are normalized by the energy present at the crossover wavenumber between dominant dissipation from crystallization versus deformation (dashed lines, Methods). Energy is input as small propagating sheets (large k) and cascades up in spatial scale through mechanical mixing and merging, with a spectral slope that depends on intrusion size.

distinguishes the dissipation regimes and depends on the thermal state of the crust and rheological parameters, with a maximum intrusion size set by crustal thickness.

If the observed distribution of intrusion sizes $N(k)$ is an accurate proxy for the self-similar energy cascade described by equation (1), we expect the total energy present at each wavenumber k to be constant. Despite the disparate crustal regions represented by our data set, this hypothesis is supported by Fig. 1b. We can choose a stress exponent n such that the product $N(k)E(k)/k$ is approximately constant over nearly the complete range of intrusion sizes (Fig. 1b, blue curve). For $k > \sim 2\,\mathrm{km}^{-1}$ we are unable to find parameters that collapse our data, suggesting that plastic or brittle deformation is governed by local processes independent of either the mantle supply or average crustal rheology, or that our third assumption breaks down for small intrusions.

Controls on the storage and eruption of mantle melts

Long-lived magmatic provinces record many generations of transport structures that alternately become active or freeze, delivering some magma to the surface and depositing the majority in the crust. If this deposited heat is not efficiently removed, crustal rocks will progressively warm and their mechanical response to inputs will evolve, in turn, to favour storage and the establishment of a reverse energy cascade. This picture provides a general framework to connect volcanic output to the evolving rheology and structure of the crust: the tendency for magma storage versus eruption is a dynamic property of crustal evolution. A young arc with De ≫ 1 (Fig. 2a), erupting at near the rate at which magma is supplied, should exhibit intrusions distributed stochastically in the range of dyke and sill thicknesses, with no energy exchange among scales. Surface eruptions will closely mimic the spatial distribution of mantle input. Monogenetic vent fields such as observed on the Colorado Plateau, USA, or distributed over the central Cascades arc, USA, are good candidates for high-De settings with different Tr.

For the same mantle supply, a longer-lived transport network with De ≪ 1 (Fig. 2b,c) will evolve to a regime of enhanced storage, and a power-law intrusion size distribution governed by a reverse energy cascade (equation (1)). Under these conditions, stress interactions[25,36] or mushy transport dynamics[4,24,37] can drive intrusion mixing and merging, such that spatial and temporal surface eruption patterns become uncorrelated with mantle inputs. High magmatic intrusive/extrusive ratios[2] are ultimately a necessary condition for the reverse energy cascade to emerge as a steady-state property of magma transfer. Commonality of ductile structures in host rocks as shallow as inferred at 5–6 km palaeodepths in arc plutonic complexes[28] suggest that near-crustal-scale De < 1 behaviour is often achieved. We suggest that volcanic centres with a record of transitioning from small events to caldera-forming eruptions, such as the Taupo volcanic zone, New Zealand, or Yellowstone, USA, reflect low-De conditions for different Tr.

Does the size distribution of plutonic intrusions provide an observational constraint for the magnitude and frequency of mantle melt influx to the crust? Sensitivity to temporal changes in the distribution and rate at which mantle melts are supplied is governed by a stirring time $T_{mix} \sim V/Q$ (ref. 38), where V is the volume of the De < 1 region (Fig. 2a,b) and Q is average mantle influx. Fluctuations expressed through changes in V imparted on timescales less than T_{mix} are subsequently modulated by intrusion merging and are not expected to be preserved in the intrusive record, although they may be recorded by crystal-scale chemical zoning or heterogeneity[39]. For $Q \sim 10^{-3}$–$10^{-2}\,\mathrm{km}^3\,\mathrm{yr}^{-1}$ we find $T_{mix} \sim 10^5$–10^6 yr, similar to variations in pluton assembly estimated through geochronology[40]. We expect some dependence of T_{mix} on intrusion depth, as suggested by observations from crustal sections[23]. Magmatic flare-ups[41] or large igneous provinces[42] that involve more spatially extensive pathways than average volcanic episodes[37] represent a type of 'system-clearing event'[43], and should by contrast be preserved if magma transport structures spanning the crust are activated, or if regional thermal weakening reaches crustal scales.

Linking mantle thermal histories with long-term climate

Our model predicts that coupling between the mantle and the surface will evolve over the life of a crustal magmatic system, as the regime of storage (Fig. 2c) modulates the erupted fraction of mantle magma supply as well as the locations and temporal frequency of surface volcanism. An evolving pattern of volcanism consequently has implications beyond the growth and differentiation of Earth's crust. In particular, modulation of deep crustal storage and surface eruptions exerts control over Earth's well-established long-term climate variability on timescales greater than about a million years[44]. Whereas the extent to which magma is stored at depths below CO_2 exsolution governs the global rate of volcanic CO_2 outgassing, on average, the resulting greenhouse forcing depends also on the recurrence interval of eruptions relative to a characteristic timescale for chemical weathering that declines with the surface area and volume of basaltic lavas emplaced at the surface[45].

For a given magma supply from the mantle and Tr, arcs may age and evolve from De ≫ 1 to De ≪ 1 conditions. This behaviour implies that eruptive outgassing as well as the strength of the chemical weathering sink for atmospheric CO_2 will reflect the shift between dominantly frequent small eruptions and very large events recurring over timescales potentially longer than typical weathering times. We suggest that the importance of comparing mantle heat and melt delivery to crustal cooling, as a control parameter for regimes of magma transport, has implications for crustal evolution and mantle–climate coupling on terrestrial planets generally. Planetary mantle convective and tectonic modes evolve in complex ways through time[44,46]. Our approach provides a framework to characterize the variable De — Tr conditions that occur during planetary thermal evolution at the largest scales and thus quantify the consequences of time-varying proclivities for magma eruption and storage.

Methods

Methods, including statements of data availability and any associated accession codes and references, are available in the online version of this paper.

Received 14 April 2017; accepted 7 June 2017; published online 10 July 2017

References

1. Crisp, J. A. Rates of magma emplacement and volcanic output. *J. Volcanol. Geotherm. Res.* **20,** 177–211 (1984).
2. White, S. M., Crisp, J. A. & Spera, F. J. Long-term volumetric eruption rates and magma budgets. *Geochem. Geophys. Geosyst.* **7,** Q03010 (2006).
3. Lee, C.-T. A., Thurner, S., Paterson, S. R. & Cao, W. The rise and fall of continental arcs: interplays between magmatism, uplift, weathering, and climate. *Earth Planet. Sci. Lett.* **425,** 105–119 (2015).
4. Cashman, K. V., Sparks, R. S. J. & Blundy, J. D. Vertically extensive and unstable magmatic systems: a unified view of igneous processes. *Science* **355,** aag3055 (2017).
5. Davidson, J., Tepley, F., Palacz, Z. & Meffan-Main, S. Magma recharge, contamination and residence times revealed by *in situ* laser ablation isotopic analysis of feldspar in volcanic rocks. *Earth Planet. Sci. Lett.* **184,** 427–442 (2001).
6. de Silva, S. L. & Gosnold, W. D. Episodic construction of batholiths: insights from the spatiotemporal development of an ignimbrite flare-up. *J. Volcanol. Geotherm. Res.* **167,** 320–335 (2007).
7. Aoki, Y., Segall, P., Kato, T., Cervelli, P. & Shimada, S. Imaging magma transport during the 1997 seismic swarm off the Izu Penninsula, Japan. *Science* **286,** 927–930 (1999).
8. Petford, N. Rheology of granitic magma during ascent and emplacement. *Annu. Rev. Earth Planet. Sci.* **31,** 399–427 (2003).
9. Wada, Y. On the relationship between dike width and magma viscosity. *J. Geophys. Res.* **99,** 17743–17755 (1994).
10. Rubin, A. M. Getting granite dikes out of the source region. *J. Geophys. Res.* **B4,** 5911–5929 (1995).
11. Krumbholz, M. *et al*. Weibull-distributed dyke thickness reflects probabilistic character of host-rock strength. *Nat. Commun.* **5,** 3272 (2014).
12. McCaffrey, K. & Petford, N. Are granitic plutons scale invariant? *J. Geol. Soc. Lond.* **154,** 1–4 (1997).
13. Annen, C. & Sparks, R. S. J. Effects of repetitive emplacement of basaltic intrusions on thermal evolution and melt generation in the crust. *Earth Planet. Sci. Lett.* **203,** 937–955 (2002).
14. Michaut, C. & Jaupart, C. Two models for the formation of magma reservoirs by small increments. *Tectonophysics* **500,** 34–49 (2011).
15. Jellinek, A. M. & DePaolo, D. J. A model for the origin of large silicic magma chambers: precursors of caldera-forming eruptions. *Bull. Volcanol.* **65,** 363–381 (2003).
16. Gerya, T. V. & Burg, J.-P. Intrusion of ultramafic bodies into the continental crust: numerical simulation. *Phys. Earth Planet. Inter.* **160,** 124–142 (2007).
17. Karlstrom, L., Dufek, J. & Manga, M. Magma chamber stability in arc and continental crust. *J. Volcanol. Geotherm. Res.* **190,** 249–270 (2010).
18. Hutton, D. H. W. & Reavy, R. J. Strike-slip tectonics and granite petrogenisis. *Tectonics* **11,** 960–967 (1992).
19. McNulty, B. A., Tong, W. & Tobisch, O. T. Assembly of a dike-fed magma chamber: the Jackass Lakes pluton, central Sierra Nevada, California. *Geol. Soc. Am. Bull.* **108,** 926–940 (1996).
20. Paterson, S., Memeti, V., Mundil, R. & Zak, J. Implications of repeated, multiscale, magmatic erosion and recycling in a mid-crustal pluton. *Am. Mineral.* **101,** 2176–2198 (2016).
21. Wiebe, R. A. Basaltic injections into floored silicic magma chambers. *EOS Trans. Am. Geophys. Union* **74,** abstr. V44C-06 (1993).
22. Vigneresse, J. L. & Bouchez, J. L. Successive granitic magma batches during pluton emplacement: the case of Cabeza de Araya (Spain). *J. Petrol.* **38,** 1767–1776 (1997).
23. Paterson, S., Okaya, D., Memeti, V., Economos, R. & Miller, R. Magma addition and flux calculations of incrementally constructed magma chambers in continental margin arcs: combined field, geochronologic, and thermal modeling studies. *Geosphere* **7,** 1439–1468 (2011).
24. Rubin, A. M. Dikes vs. diapirs in viscoelastic rock. *Earth Planet. Sci. Lett.* **117,** 653–670 (1993).
25. Karlstrom, L., Dufek, J. & Manga, M. Organization of volcanic plumbing through magmatic lensing by magma chambers and volcanic edifices. *J. Geophys. Res.* **114,** B006339 (2009).
26. Galland, O., Burchardt, S., Hallot, E., Mourgues, R. & Bulois, C. Dynamics of dikes versus cones sheets in volcanic systems. *J. Geophys. Res.* **119,** 6178–6192 (2014).
27. Townsend, M. R., Pollard, D. D. & Smith, R. P. Mechanical models for dikes: a third school of thought. *Tectonophysics* **703,** 98–118 (2017).
28. Miller, R. B. & Paterson, S. R. Construction of mid-crustal sheeted plutons: examples from the North Cascades, Washington. *Geol. Soc. Am. Bull.* **113,** 1423–1442 (2001).
29. Cathles, L. M. An analysis of the cooling of intrusives by ground-water convection which includes boiling. *Econom. Geol.* **72,** 804–826 (1977).
30. Rubie, D. C. Reaction-enhanced ductility: the role of solid-solid univariant reactions in deformation of the crust and mantle. *Tectonophysics* **96,** 331–352 (1983).
31. Kirby, S. H. & Kronenberg, A. K. Rheology of the the lithosphere: selected topics. *Rev. Geophys.* **25,** 1219–1244 (1987).
32. Menand, T., Annen, C. & de Saint Blanquat, M. Rates of magma transfer in the crust: insights into magma reservoir recharge and pluton growth. *Geology* **43,** 199–202 (2015).
33. Petford, N. & Gallagher, K. Partial melting of mafic (amphibolitic) lower crust by periodic influx of basaltic magma. *Earth Planet. Sci. Lett.* **193,** 483–499 (2001).
34. Kolmogorov, A. N. The local structure of turbulence in incompressible viscous fluid for very large Reynolds numbers. *Proc. USSR Acad. Sci.* **30,** 9–13 (1941).
35. England, P. & McKenzie, D. A thin viscous sheet model for continental deformation. *Geophys. J. Int.* **70,** 295–321 (1982).
36. Weinberg, R. F. Mesoscale pervasive felsic magma migration: alternatives to dyking. *Lithos* **46,** 393–410 (1999).
37. Christopher, T. E. *et al*. Crustal-scale deagssing due to magma system destabilization and magma-gas decoupling at Soufreiére Hills Volcano, Montserrat. *Geochem. Geophys. Geosyst.* **16,** 2797–2811 (2015).
38. Jerolmack, D. J. & Paola, C. Shredding of environmental signals by sediment transport. *Geophys. Res. Lett.* **37,** L044638 (2010).
39. Kent, A. J. R., Darr, C., Koleszar, A. M., Salisbury, M. J. & Cooper, K. M. Preferential eruption of andesitic magmas through recharge filtering. *Nat. Geosci.* **3,** 631–636 (2010).
40. Matzel, J. E. P. & Bowring, S. A. Time scales of pluton construction at differing crustal levels: examples from the Mount Stuart and Tenpeak intrusions, North Cascades, Washington. *GSA Bull.* **118,** 1412–1430 (2006).
41. Ducea, M. N., Paterson, S. R. & Decelles, P. G. High-volume magmatic events in subduction systems. *Elements* **11,** 99–104 (2015).
42. Bryan, S. E. & Ferrari, L. Large igneous provinces and silicic large igneous provinces: progress in our understanding over the last 25 years. *Geol. Soc. Am. Bull.* **125,** 1053–1078 (2013).
43. Bak, P., Tang, C. & Wiesenfeld, K. Self-organized criticality - an explanation for 1/f noise. *Phys. Rev. Lett.* **59,** 381–384 (1987).
44. Lenardic, A., Jellinek, A. M., Foley, B., O'Neill, C. & Moore, W. B. Climate-tectonic coupling: variations in the mean, variations about the mean, and variations in the mode. *J. Geophys. Res.* **121,** 1831–1864 (2016).
45. Dessert, C. *et al*. Erosion of Deccan Traps determined by river geochemistry: impact on the global climate and the $^{87}Sr/^{86}Sr$ ratio of seawater. *Earth Planet. Sci. Lett.* **188,** 459–474 (2001).
46. Jellinek, A. M. & Jackson, M. G. Connections between the bulk composition, geodynamics and habitability of Earth. *Nat. Geosci.* **8,** 587–593 (2015).
47. Ray, R., Sheth, H. C. & Mallik, J. Structure and emplacement of the Nandurbar-Dhule mafic dyke swarm, Deccan Traps, and the tectonomagmatic evolution of flood basalts. *Bull. Volcanol.* **69,** 537–551 (2007).
48. Muirhead, J. D., White, G. A. J. D. L. & Rowland, J. V. Cracking the lid: sill-fed dikes are the likely feeders of flood basalt eruptions. *Earth Planet. Sci. Lett.* **406,** 187–197 (2014).

Acknowledgements

L.K. and S.R.P. acknowledge support from NSF. L. Vanderkluysen provided Deccan Traps dyke thickness data.

Author contributions

L.K. and A.M.J. conceived the study, developed the model and wrote the paper. S.R.P. compiled plutonic intrusion size data and provided critical input related to field observations. L.K. carried out all calculations.

Additional information

Supplementary information is available in the online version of the paper. Reprints and permissions information is available online at www.nature.com/reprints. Publisher's note: Springer Nature remains neutral with regard to jurisdictional claims in published maps and institutional affiliations. Correspondence and requests for materials should be addressed to L.K.

Competing financial interests

The authors declare no competing financial interests.

Methods

Field constraints on intrusion growth and measurements of intrusion sizes. A substantial literature of chemical, geochronological and structural studies establishes the observational basis for our study. The primary observations that support development of the reverse energy cascade model are the well-defined internal contacts between distinct plutonic intrusive bodies that have been established by refs 21,49–54 among many others. Evidence that smaller bodies merge into larger bodies is widespread and may be found in, for example, refs 19,23,28,55–59.

The data supporting the findings of our study are available within the article and its Supplementary Information. Our database of measured pluton shapes and sizes comes from analyses of new and published geologic maps of Mesozoic arc sections in the North American Cordillera from: the Cascades crystalline core, Washington; the central Sierra Nevada, California; the northern Peninsular Ranges Batholith in southern California and northern Baja California; and the Transverse Ranges and a tilted crustal section in the Joshua Tree area, Mojave Desert, California. We focus on macro-scale morphology classified on the basis of mapped contacts, age, mineralogy, geochemistry and internal structures.

For each plutonic body, the length, thickness (longest and shortest dimensions in map view) and, where possible, width (dimension perpendicular to plane of length and thickness[60]) were measured. Supplementary Fig. 1 illustrates these measurements for the Zarza pluton, Baja California, Mexico[57]. Areas were calculated both from length and thickness determinations and are similar to independent estimates from areas of enclosed polygonal shapes. In tilted crustal sections, the map pattern provides length and width estimates and thickness must be estimated. For example, local topography, exposures of exhumed different crustal depths, and the tilted crustal section in the Joshua Tree area provide some control on vertical dimensions. Supplementary Fig. 2 plots length and thickness from our data set along with a proposed power-law scaling derived from different data[60]. Area/volume estimates scale self-consistently to the total composite pluton size. We do not attempt to further refine the data set here by intrusion crystallization depth, although the crustal sections represented here do exhibit structural variation with depth[61].

Special focus was given to ten intrusive complexes where detailed maps, combined with geochronologic and geochemical data sets, provide a measure of completeness, genetic relationships and total size. This allows us to quantify the number density of intrusions. The smallest pulse size is arbitrarily set by current field measurements, although the true size distribution extends down to the scale of crystal aggregations[62]. Characterizing the primary size distribution of frozen intrusions remains challenging due to poor constraints on the depth extent, incomplete preservation and sometimes ambiguous internal contacts. Intermediate- and large-scale plutonic bodies are directly measured, but the large number of thin sheets present in heterogeneous complexes[23] makes individual measurements challenging. Instead, average dimensions were determined for intrusive bodies with wavenumbers $k \geq 1\,\mathrm{km}^{-1}$ and the total number of intrusions estimated by dividing the total sheeted area by average individual sheet area. Future mapping will refine the large k limit of this distribution, and we consider the relation $N(k)$ between number of intrusions and wavenumber in Fig. 1b a preliminary result. However, the key observation that orders of magnitude more small bodies are present is robust.

Timescales for a crustal-scale rheological transition. To satisfy the three main assumptions stated in the text for an energy cascade, a large-scale rheological transition must occur. We estimate the time required to trigger a crustal-scale rheological transition driven by crystallizing intrusions with a one-dimensional thermal model. Mafic dykes are assumed to be the primary input of magma into the crust, occurring stochastically in time and space but with enough regularity that a long-term mean flux rate[63] can be defined, as well as a variability around this mean[64]. We model influx variations in bulk, fixing the average influx Q_{in0} but allowing this to be distributed as regular sinusoidal pulses described by the positive part of:

$$Q_{\mathrm{in}} = Q_{\mathrm{in0}}\pi \sin(2\pi t/T_{\mathrm{supply}}) \tag{2}$$

where T_{supply} is the period of mantle melt variability. Scaling this timescale by a diffusion time $T_{\mathrm{diffusion}} = (h/2)^2/\kappa$, where h is the vertical scale over which Q_{in} is uniformly distributed ($h <$ crustal thickness z_{crust}) and κ is a thermal diffusivity, gives the transport number $\mathrm{Tr} = T_{\mathrm{supply}}/T_{\mathrm{diffusion}}$ plotted in Fig. 2c. We use half the vertical extent of dyking $h/2$ as a scale length for diffusion within the intruded zone of the crust.

The emplacement and cooling of dykes provide a heat source in the crust of magnitude $H_{\mathrm{dyke}}(t) = F\rho(c_{\mathrm{p}}\Delta\theta + L)q_{\mathrm{in}}(t)/h$, where c_{p} is the specific heat capacity, $\Delta\theta = \theta_l - \theta(z,t)$ is the temperature of the emplaced magma (liquidus $\theta_l = 1{,}100\,\mathrm{C}$) relative to host rocks (at temperature $\theta(z,t)$ that is a function of time t and depth z), and $L = 310\,\mathrm{kJ\,kg}^{-1}$ is the latent heat of fusion. The influx per area is $q_{\mathrm{in}}(t) = Q_{\mathrm{in}}(t)/z_{\mathrm{crust}}^2$. Some of the heat input through intrusions exits the crust via eruptions, or is advected away from the intrusion by fluids. We include a dimensionless eruption efficiency $F = 0.01$ as a model for this process. The thermal regime of the crustal volume then evolves as:

$$\rho c_{\mathrm{p}}\frac{\partial\theta}{\partial t} = k_{\mathrm{c}}\frac{\partial^2\theta}{\partial z^2} + H_{\mathrm{rad}} + H_{\mathrm{dyke}}(t)d(z) \tag{3}$$

with density ρ and thermal conductivity k_{c}. $H_{\mathrm{rad}} = \mathrm{e}^{-z/h_{\mathrm{r}}}(W_{r0} - W_{\mathrm{rm}})/h_{\mathrm{r}}$ is the rate of radiogenic heat production in the crust as a function of depth constrained by surface heat flux W_{r0}, mantle heat flux W_{rm}, and decay constant h_{r}. We use dimensionless $d(z) = 1/2(1 + \tanh[10(z-h)/z_{\mathrm{crust}}])$ to model the localized heating in a region with a specified vertical scale h above the base of the crust z_{crust}.

Equation (3) involves a poorly constrained prescription of vertical intrusion distribution and heating efficiency, but still captures the essential physics on a large scale: intrusions heat up relatively insulating, conductive host rocks through time[65]. Supplementary Fig. 3a plots a solution to equation (3), assuming an initially steady-state geotherm, for $k_{\mathrm{c}} = 2\,\mathrm{W\,m}^{-1}\,\mathrm{K}^{-1}$, $c_{\mathrm{p}} = 1{,}200\,\mathrm{J\,kg}^{-1}\,\mathrm{K}$, $h_{\mathrm{r}} = 10\,\mathrm{km}$, $W_{r0} = 45\,\mathrm{mW\,m}^{-2}$, $W_{\mathrm{rm}} = 20\,\mathrm{mW\,m}^{-2}$, $\rho = 2{,}600\,\mathrm{km\,m}^{-3}$, with intrusions spanning $h = 15\,\mathrm{km}$ and $z_{\mathrm{crust}} = 30\,\mathrm{km}$ taken as representative values for arc crust. For this calculation, we assume that the period of influx variability T_{supply} is short, so influx is steady in time, $Q_{\mathrm{in0}} = 10^{-3}\,\mathrm{m}^3\,\mathrm{yr}^{-1}$, and heating is diffusion-limited.

We now estimate the effect of background crustal heating on an individual intrusion that is much smaller than the size of the crustal volume. The mechanical evolution of any of these hydraulically isolated melt pockets is assumed to follow a Maxwell viscoelastic constitutive law relating increments of volumetric strain ϵ arising from injection of magma to a total stress σ as $\dot{\epsilon} = \dot{\sigma}/E + \sigma/\mu$, where $E = 10\,\mathrm{GPa}$ is a local elastic modulus and μ is a local host-rock viscosity. Force balance at the magma/rock interface dictates that deviations from lithostatic stress in the rocks will arise from dynamic pressures and buoyancy; we lump both into an overpressure and consider only volumetric deformation. Pressure changes over time then depend on the rate at which elastic stresses are relaxed:

$$\frac{1}{K}\frac{\mathrm{d}\hat{P}}{\mathrm{d}t} = \frac{\left(\hat{Q}_{\mathrm{in}} - \hat{Q}_{\mathrm{out}}\right)}{\hat{V}_{\mathrm{c}}} - \frac{\hat{P}}{\mu} \tag{4}$$

where volumetric strains are associated with recharge and eruption $(\hat{Q}_{\mathrm{in}} - \hat{Q}_{\mathrm{out}})/\hat{V}_{\mathrm{c}}$ with $\hat{V}_{\mathrm{c}}$ an intrusion volume, and an effective elastic modulus K incorporates both magma and chamber compressibility[66]. The outflux by eruption $\hat{Q}_{\mathrm{out}}$ is non-zero only when $\hat{P} > P_{\mathrm{c}}$, the maximum overpressure that can be sustained by crustal rocks[10]. Hatted variables represent quantities associated with an individual intrusion (rather than a crustal volume). The dynamics of equation (4) are well known[15], governed by a Deborah number $\mathrm{De} \sim (\mu\hat{Q}_{\mathrm{in}})/(V_0 K)$ that measures the timescale of Maxwell viscoelastic stress relaxation ($T_{\mathrm{relax}} \sim \mu/K$), to a typical inverse strain rate ($T_{\mathrm{inject}} \sim V_0/\hat{Q}_{\mathrm{in}}$). We assume box-like intrusions uniformly 0.5 m in width and that span the intrusion domain h to calculate V_0. If $\mathrm{De} \gg 1$, the chamber exhibits an elastic response to influx: it fills until pressure reaches the maximum overpressure P_{c} then ruptures and drains, leading to cycles of eruptions for prolonged influx[67]. If $\mathrm{De} \ll 1$, the wall rocks viscously dissipate any excess pressure, leading to magma storage and intrusion growth.

We use the temperature field from equation (3) to estimate the evolving viscosity of the crust, assuming an Arrhenius law to explore the role of temperature on average viscosity $\mu = A_\mu \exp G_\mu/(R\theta)$ with empirical constants A_μ, G_μ and gas constant R (to be distinguished from the explicitly stress-dependent case discussed in the next section). Supplementary Fig. 3b,c illustrates the evolution of crustal viscosity for Westerly Granite[15], and the subsequent evolution of the Deborah number De as crustal viscosity decreases. We shut off the simulation when $\mathrm{De} = 1$ at the top of the intrusion region (in this case it takes 200 kyr). It can be seen that $\mathrm{De} < 1$ even for a normal geotherm at depths below 25 km, a lower crust generally ductile with respect to magmatism.

Supplementary Fig. 4 then explores a range of average influx rates Q_{in0} and spatial extents of magmatic heating h through dykes, to explore likely intrusion scenarios and mantle inputs. We focus on diffusion-limited heating ($\mathrm{Tr} \ll 1$) here, with variable mantle influx at fixed Q_{in0} plotted in Fig. 2c of the main text. Thermal modelling[32,68] suggests that $Q_{\mathrm{in0}} \sim 10^{-3} - 10^{-2}\,\mathrm{km}^3\,\mathrm{yr}^{-1}$ is necessary to build large, long-lived intrusions incrementally, which is similar to the magma budget estimated for arc environments[2]. As demonstrated by Supplementary Fig. 4, the time required to reach $\mathrm{De} = 1$ for a large column of crust is thus probably tens to hundreds of thousands of years.

Derivation of scaling laws for dissipation. We postulate that the distribution of intrusion sizes observed in thermally evolved ($\mathrm{De} \ll 1$ regime) magmatic provinces is a consequence of self-similar energy transfer among scales. This energy transfer may be quantified by an energy balance for crustal volume V that contains a mixture of host rocks and magmatic intrusions with a range of temperatures and melt fractions:

$$\rho\frac{\partial U}{\partial t} = -\nabla\cdot\left(q_{\mathrm{c}} + \rho U\mathbf{v}\right) + (\nabla\cdot\mathbf{v})(\rho U - P) - \tau : \nabla\mathbf{v} + \rho\left(\dot{U}_{\mathrm{in}} - \dot{U}_{\mathrm{out}}\right) \tag{5}$$

Here $U = c_p\Delta\theta + Lf$ is internal energy per unit mass for the partially molten mixture with f being the local melt fraction, $q_c = -k_c\nabla\theta$ is the conductive heat flux, P is pressure, τ is the deviatoric stress tensor, $\mathbf{v}$ is a velocity vector specifying a distribution of motions of the liquid melt and solid matrix mixture, and $\dot{U}_{in} - \dot{U}_{out}$ is the net input of internal energy.

The magmatic energy cascade refers to a statistically steady-state local transfer of energy among intrusion scales. Heat transfer by conduction does not involve the creation of new physical intrusion scales so does not participate directly in the cascade, although it is critically important for the evolving rheological response of crustal rocks that governs mechanical dissipation. We neglect sinks of energy through eruptions $\dot{U}_{out}$. The distribution of intrusion scales is then governed by mass transfer within the volume, for example, by terms in equation (5) involving $\mathbf{v}$.

The divergence of mixture velocity $\nabla\cdot\mathbf{v}$ accounts for volumetric work done to the crustal volume through opening intrusions (crustal rocks and magma are nearly incompressible unless volatiles exsolve). In the $\mathrm{De} \ll 1$ limit, these terms are negligible because volume change is accommodated by crustal flow. Transfer of energy between scales for intrusions within V involves two sources of energy dissipation that we label by Φ_M and Φ_T, the sum of which is:

$$\Phi = \Phi_T + \Phi_M = \nabla\cdot(\rho U\mathbf{v}) + \tau:\nabla\mathbf{v} \tag{6}$$

We do not consider the distribution of mass transfer and deformation within V here, but rather use scaling to estimate Φ_M and Φ_T. The contribution of mechanical dissipation (assuming stored elastic energy is negligible) follows from modelling crustal materials as a pseudo-plastic power-law fluid, for which strain rate $\dot{\epsilon}$ scales with deviatoric stress τ as:

$$\dot{\epsilon} = A_c\tau^n \exp\left[G_c/(R\theta)\right] \tag{7}$$

with A_c and G_c being empirical constants[69]. Dissipated mechanical energy Φ_M is then:

$$\Phi_M = \tau:\dot{\epsilon} \sim \dot{\epsilon}^{\frac{1}{n}+1} \tag{8}$$

Φ_M approaches a linear relationship with $\dot{\epsilon}$ as the exponent n increases and stress becomes less and less sensitive to strain rate. As $n\to 1$, Φ_M approaches the Newtonian viscous limit and applied stresses produce deformations over length scales comparable to k^{-1}. As n grows, the crust behaves increasingly as a perfect plastic (approximating brittle behaviour), with deformation concentrated in thin zones[35,70] with thicknesses much smaller than k^{-1}. For the crust, $n\sim 2-10$, with larger exponents to model shear zones[71] and lower exponents from experiments on crustal rocks[69].

If deformation is dominated by magmatic recharge to intrusions subject to constant volumetric influx similar to Q_{in} then the strain rate is $\dot{\epsilon}\sim Q_{in}k^3$, where k is the characteristic intrusion wavenumber. Dissipation then scales as $\Phi_M \sim C_M k^{3((1/n)+1)}$, with C_M independent of wavenumber. This mechanical dissipation rate is larger for smaller intrusions: for fixed Q_{in}, strain rate decreases rapidly as k decreases.

The other contribution to dissipation, Φ_T, involves advection of internal energy (dominated by the latent heat of fusion) within the crustal volume. Over sufficiently long timescales, heat transfer is supply limited and heat flux tracks variations in melt influx[33] as generations of intrusions crystallize. We assume that interactions among scales (for example, dyke interactions or magma chamber lensing of dykes[25]) efficiently spread mantle melt influx throughout the crustal volume, so $\mathbf{v}\sim q_{in}$. In such a case the heat flux $U\mathbf{v}$ should be[14]:

$$U\mathbf{v} \sim q_{in}\rho(c_p\Delta\theta + L) \tag{9}$$

The intrusion scale length is k^{-1}, so $\Phi_T = \nabla\cdot(U\mathbf{v}) \sim C_T k$ with C_T independent of wavenumber.

The energy spectrum for intrusions (energy per wavenumber k) may now be estimated from dimensional analysis. If we assume that energy transfer between scales is self-similar, the quantities that determine energy E present per wavenumber are the dissipation rate, integrated over the crustal volume and wavenumber. The integral over volume is independent of wavenumber; thus, $E(k)/k \sim \Phi(k)^a k^b$, with $a = 2/3$ and $b = -5/3$ for dimensional consistency. If Φ is independent of k, this is the Kolmogorov 'five-thirds' scaling law[34]. The regimes of dissipation discussed above suggest the following scaling:

$$\frac{E(k)}{k} \sim \Phi(k)^{2/3}k^{-5/3} \sim \left(C_M k^{3(\frac{1}{n}+1)} + C_T k\right)^{2/3} k^{-5/3} \tag{10}$$

In the limit that $C_T/C_M \gg 1$, equation (10) gives an inverse spectrum for $E(k)/k \sim k^{-1}$, whereas the limit of $C_T/C_M \ll 1$ gives $E(k)/k \sim k^{1/3+2/n}$, for which large wavenumbers dominate. The crossover wavenumber is:

$$k_{crit} = \left(\frac{C_M}{C_T}\right)^{-1/(2+\frac{3}{n})} = \left(\frac{\left[q_{in}A_c\exp(G_c/(R\theta))\right]^{\frac{1}{n}} z_{crust}^{\frac{1}{n}+1}}{\rho(c_p\Delta\theta + L)}\right)^{-1/(2+\frac{3}{n})} \tag{11}$$

For reasonable parameter values, $k_{crit}^{-1} \sim 10\text{s}–500\text{s}$ m. The existence of two regimes for $\mathrm{De} < 1$ (and hence a crossover wavenumber) may be understood through analogy to the dynamics of a single intrusion described by equation (4). The timescale for crystallization of an intrusion of scale k^{-1} scales as $\sim \rho U/(k\Theta_S) \propto k^{-1}$, where Θ_S is the heat flux at the surface of the intrusion. Deformation timescales scale with inverse strain rate as $\sim V_0/Q_{in} \propto k^{-3}$. The shortest timescale dominates: deformation times are shorter at high k associated with mantle input, but as $k\to 0$ during the energy cascade, crystallization rates will eventually become shorter.

Code availability. The Matlab code used for the model is provided in the Supplementary Information.

Data availability. Raw plutonic data are provided in the Supplementary Information. Raw dyke data are available from refs 11,47,48. Additional Deccan Traps data come from L. Vanderkluysen by request.

References

49. Wager, L. R. & Brown, G. M. *Layered Igneous Rocks* (Oliver and Boyd, 1967).
50. Irvine, T. N. Terminology for layered intrusions. *J. Petrol.* **23,** 127–162 (1982).
51. Cawthorn, R. G. *Layered Intrusions* (Elsevier, 1996).
52. Zak, J. & Paterson, S. R. Characteristics of internal contacts in the Tuolumne Batholith, central Sierra Nevada, California (USA): implications for episodic emplacement and physical processes in a continental arc magma chamber. *GSA Bull.* **117,** 1242–1255 (2005).
53. Paterson, S. R., Zak, J. & Janousek, V. Growth of complex magmatic zones during recycling of older magmatic phases: the Sawmill Canyon area in the Toulumne Batholith, Sierra Nevada, California. *J. Volcanol. Geotherm. Res.* **177,** 457–484 (2008).
54. Miller, C. F. *et al*. Growth of plutons by incremental emplacement of sheets in crystal-rich host: evidence from Miocene intrusion of the Colorado River region, Nevada, USA. *Tectonophysics* **500,** 65–77 (2011).
55. Hardee, H. C. Incipient magma chamber formation as a result of repetitive intrusions. *Bull. Volcanol.* **45,** 41–49 (1982).
56. Lagarde, J. L., Brun, J. P. & Gapais, D. Formation of epizonal granitic plutons by *in situ* assemblage of laterally expanding magma. *Adadémie des Sci. Comptes Rednus* **310,** 1109–1114 (1990).
57. Johnson, S. E., Paterson, S. R. & Tate, M. C. Structure and emplacement history of a multiple-center, cone-sheet-bearing ring complex: the Zarza Intrusive Complex, Baja California, Mexico. *Geol. Soc. Am. Bull.* **111,** 607–619 (1999).
58. Lipman, P. W. Incremental assembly and prolonged consolidation of Cordilleran magma chambers: evidence from the Southern Rocky Mountain volcanic field. *Geosphere* **3,** 42–70 (2007).
59. Michel, J., Baumgartner, L., Putliz, B., Schaltegger, U. & Ovtcharova, M. Incremental growth of the Patagonian Torres del Paine laccolith over 90 k.y. *Geology* **36,** 459–462 (2008).
60. Cruden, A. R. & McCaffrey, K. J. W. Growth of plutons by floor subsidence: implications for rates of emplacement, intrusion spacing and melt-extraction mechanisms. *Phys. Chem. Earth A* **26,** 303–315 (2001).
61. Miller, R. B., Patterson, S. R. & Matzel, J. P. Plutonism at different crustal levels: insights from the ~5-40 km (paleodepth) North Cascades crustal section, Washington. *Geol. Soc. Am. Spec. Pap.* **456,** 125–149 (2009).
62. Vernon, R. H. & Paterson, S. R. Mesoscopic structures resulting from crystal accumulation and melt movement in granites. *Trans. R. Soc. Edinburgh* **97,** 369–381 (2006).
63. Dufek, J. & Bergantz, G. W. Lower crustal magma genesis and preservation: a stochastic framework for the evaluation of basalt-crust interaction. *J. Petrol.* **46,** 2167–2195 (2005).
64. Schöpa, A. & Annen, C. The effects of magma flux variations on the formation and lifetime of large silicic magma chambers. *J. Geophys. Res.* **118,** 1–17 (2013).
65. Carrigan, C. R. Biot number and thermos bottle effect: implications for magma-chamber convection. *Geology* **16,** 771–774 (1988).
66. Segall, P. *Earthquake and Volcano Deformation* (Princeton, 2010).
67. Degruyter, W. & Huber, C. A model for eruption frequency of upper crustal silicic magma chambers. *Earth Planet. Sci. Lett.* **403,** 117–130 (2014).
68. Annen, C. From plutons to magma chambers: thermal constraints on the accumulation of eruptible silicic magma in the upper crust. *Earth Planet. Sci. Lett.* **284,** 409–416 (2009).
69. Bürgmann, R. & Dresen, G. Rheology of the lower crust and upper mantle: evidence from rock mechanics, geodesy, and field observations. *Annu. Rev. Earth Planet. Sci.* **36,** 531–567 (2008).
70. Jellinek, A. M., Gordon, R. G. & Zatman, S. Experimental tests of simple models for the dynamics of diffuse oceanic plate boundaries. *Geophys. J. Int.* **164,** 624–632 (2006).
71. Regenauer-Lieb, K. & Yuen, D. A. Modeling shear zone in geological and planetary sciences: solid- and fluid-thermal-mechanical approaches. *Earth-Sci. Rev.* **63,** 295–349 (2003).